X-ray Induced Photocurrents at the Metal/Solution Interface

ARTICLE *in* THE JOURNAL OF PHYSICAL CHEMISTRY B · JULY 2000

Impact Factor: 3.3 · DOI: 10.1021/jp000312o

3 AUTHORS, INCLUDING:

Yuriy Tolmachev
Ftorion
69 PUBLICATIONS **1,009** CITATIONS

SEE PROFILE

X-ray Induced Photocurrents at the Metal/Solution Interface

Yuriy V. Tolmachev, In Tae Bae, and Daniel A. Scherson

Department of Chemistry and Ernest B. Yeager Center for Electrochemical Sciences, Case Western Reserve University, Cleveland, Ohio 44106-7078

Received: January 27, 2000; In Final Form: May 7, 2000

A technique is herein described for the acquisition of X-ray absorption spectra of electrodes fully immersed in an electrolyte solution by monitoring the energy dependence of X-ray induced photocurrents. This novel strategy made it possible to obtain in situ Au L_{III}-edge X-ray absorption spectra of solid Au electrodes displaying virtually identical features to those recorded *simultaneously* via X-ray fluorescence. The dependence of the X-ray induced photocurrents on chopping frequency and electrode potential was found to be consistent with a temperature modulation of the rate of the interfacial electron transfer (faradaic heating currents), rather than electron photoemission, as the primary source of the observed effects.

Introduction

The development and implementation of spectroscopic and structural probes of condensed-phase interfaces may be expected to have pronounced impact in areas of fundamental and technological importance, including adhesion, corrosion and a variety of electrochemical phenomena. Methods that rely on tunable, high-intensity X-ray sources hold extraordinary promise for the study of such interfaces. In particular, the photon energies associated with element-specific, core−electron excitations of moderate to high atomic number elements, are, in many instances, sufficiently large to penetrate rather deeply into matter, and surface specificity can be achieved by using anomalous surface scattering,[1,2] external total reflection at grazing incidence angles[3,4] and/or electron yield (EY) detection.[5] The latter technique relies on the emission of electrons following photon absorption, which can then be detected either under vacuum or high pressure conditions utilizing an externally applied electric field to prevent electron recapture by the emitting source and to increase the collector current as in conversion electron yield (CEY) X-ray absorption spectroscopy (XAS). The lifetime of excess electrons in condensed media is short and, therefore, implementation of EY detection for condensed-phase interfaces requires at least one of the constituent phases to be thin enough for electrons to escape into the gas phase. Such conditions have been realized in the case of solid−liquid interfaces by partial emersion of electrodes from the electrolyte enabling photoemitted electrons to cross the thin layer of electrolyte into the detector placed directly above the solution.[4]

A different approach for the measurement of sustained photocurrents, developed in the field of UV−visible photoelectron emission at electrode−solution interfaces, involves the use of electron scavengers in the ionically conducting media. As explained in detail elsewhere,[6−8] electrons at the Fermi level of the electrode are excited by UV−visible radiation into the conduction band of the solvent, undergoing subsequent thermalization and solvation in the ps time scale. Solvated electrons localized a few nanometers away from the surface can then diffuse back and be recaptured by the electrode within tens of nanoseconds.[6,7] The main role of scavengers is to react with such electrons, yielding products that cannot be reoxidized at the electrode, thereby preventing the return of the photoemitted charge. Somewhat surprisingly, this elegant and potentially powerful detection scheme has not as yet been attempted for the acquisition of in situ XAS spectra.

This paper describes an experimental approach for the acquisition of XAS spectra of fully immersed electrodes originally conceived to exploit this scavenging scheme. As will be shown, implementation of this technique made it possible to obtain in situ Au L_{III}-edge XAS spectra of solid Au electrodes displaying virtually identical features to those recorded *simultaneously* via X-ray fluorescence yield. More detailed studies of the X-ray induced photocurrents, however, revealed a behavior that could not be explained by electron photoemission but was instead largely consistent with heating as primarily responsible for the observed effects.

Experimental Section

Gold was selected for these initial studies because of its large electrochemical potential window,[9] and also because photons with energies about Au L_{III}-edge (E_{edge}), i.e., 11 919 eV, can penetrate through the solution without significant attenuation. Furthermore, Au has been recently examined by gas-phase CEY-XAS,[10] allowing comparisons to be made with the results to be presented in this work. Persulfate was chosen as the scavenger, a species that may allow a doubling of the photocurrent via the following reaction sequence:

$$S_2O_8^{2-} + e_s^- = SO_4^{2-} + SO_4^{\bullet -}$$

$$SO_4^{\bullet -} + e_m^- = SO_4^{\bullet 2-}$$

where e_s^- represents an electron in solution and e_m^- an electron in the metal electrode. The overall experimental arrangement employed in these studies is shown schematically in Figure 1. The electrochemical cell comprises a bent Au wire working electrode cast in epoxy resin exposing an area 0.5×5 mm^2 to the aqueous electrolyte, placed in front of an X-ray transparent Kapton window at a distance of ca. 1 mm. A Au foil and a saturated calomel (SCE) were used as counter and reference electrodes, respectively. Except where otherwise noted all solutions were deaerated by purging with nitrogen. A PAR 173 potentiostat/galvanostat was employed to control the potential

10.1021/jp000312o CCC: $19.00
Published on Web 07/19/2000

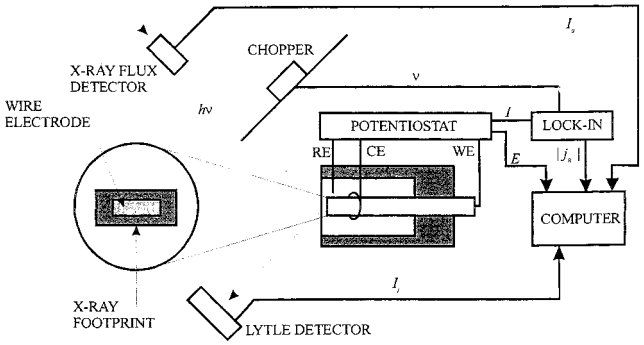

Figure 1. Schematic diagram of the experimental arrangement for recording simultaneously in situ fluorescence and photocurrent action X-ray absorption spectra. Some of the relative dimensions have been changed for clarity.

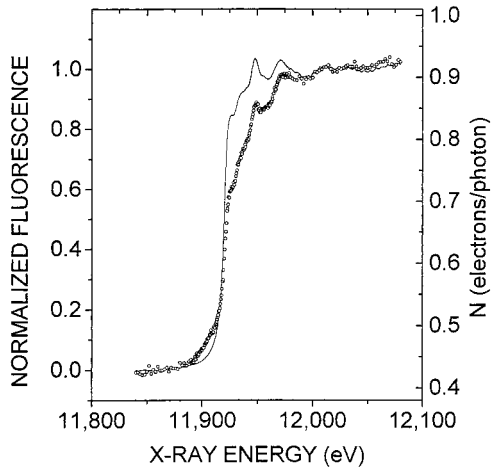

Figure 2. Fluorescence yield (solid line) and photocurrent action (open circles) spectra of the gold wire electrode in a solution 0.25 M sodium phosphate buffer (pH 6.73) + 0.25 M sodium persulfate, at 0.50 V vs SCE, recorded *simultaneously*. Chopping frequency: 6.1 Hz.

of the Au wire and also to measure the current. As indicated in the diagram, the overfilling, p-polarized X-ray beam (SSRL, beamline 4-3, photon flux ca. 2×10^9 photon/s·mm^2) was incident on the front of the electrode enabling both photocurrent and fluorescence spectra to be recorded *simultaneously* by placing a Lytle detector at 45° with respect to the normal to the surface. The X-ray beam was modulated with a mechanical chopper (Scitec Instruments, 1 mm thick brass blade) to extract the small photon-induced ac currents (picoamps to nanoamps), from a much larger dc background (nanoamps to microamps), using an SRS SR830 lock-in amplifier (Stanford Research Instruments). The overall experiment was designed so as to minimize shunting of the photocurrent through the faradaic resistance (R_{far}) and interfacial double layer capacitance (C), and, thus, increase the magnitude of the observed photocurrent in the detection circuit.[6,8]

Similar measurements involving a vapor deposited gold film on Melinex working electrode (ca. 30 nm thick, 1×5 mm^2 area) were performed at NSLS, beamline X23A, with the X-ray beam, in this case, incident from the rear of the electrode. Although of lower signal-to-noise ratio, the results obtained with such an arrangement were qualitatively similar to those found with the wire and will not be discussed further in this work.

Results and Discussion

Figure 2 shows XAS spectra of the Au wire electrode polarized at a potential of 0.50 V vs SCE in the region 11 840−12 075 eV, i.e., about the Au L_{III} edge, in a solution 0.25 M sodium phosphate buffer (pH 6.73) + 0.25 M sodium persulfate, recorded *simultaneously* in the photocurrent (circles, right ordinate) and X-ray fluorescence (solid line, left ordinate) modes at a chopping frequency, $\nu = 6.1$ Hz. The latter is plotted in terms of the effective number of photoelectrons per incident photon, $N = j_{ph}/(eI_0)$, where j_{ph} is the root-mean-square (rms) detected photocurrent, e the electron charge, and I_o is the number of photons incident on the electrode per second corrected for the absorption by the solution.

As can be clearly seen, the N vs photon energy plot, or photocurrent action (PCA) spectra, shares remarkable similarities with the more conventional fluorescence yield spectrum, including the main absorption edge and the finer features above E_{edge}. It becomes evident from these results that the photocurrent is largely derived from X-ray absorption by Au and not from other sources, such as solution phase radiolysis.[11] However, the PCA spectra displayed much larger distortions, both in the shapes and relatively intensities of the various features, compared to those recorded in fluorescence. In fact, the latter is itself distorted with respect to spectra obtained in transmission or EY due to self-absorption effect.[5,10,11−14] It is significant to note that the distortions in the PCA spectra in Figure 2 are far less pronounced than those observed for the Au L_{III}-edge spectrum acquired by CEY at high gas pressures (20 atm).[10] Also to be emphasized is the fact that photocurrents about one to 2 orders of magnitude smaller than those shown in Figure 2 could also be observed without persulfate in the solution under otherwise identical conditions (vide infra).

On the basis of the results of a number of independent PCA experiments, the edge jump ratio (EJR), i.e., unnormalized signal above E_{edge} divided by the corresponding signal below E_{edge}, varied between 1.5 and 2.5, regardless of whether persulfate was added to the media and, thus, was close to the reported photoelectric absorption cross-section jump ratio, i.e., 2.44.[15] This finding may seem surprising, as the amplification of the Auger electron current via water ionization is expected to elicit a considerable increase in the photocurrent above E_{edge}. For example, each Au LMM Auger electron emitted above the edge, which has an energy of ca. 5.5 keV, could ionize water losing ca. 12 eV per each electron ion pair produced[16] and, thereby, increase j_{ph} by a factor of several hundreds. Yet, our findings seem in line with the results of the CEY study of the same system.[10]

Measurements in which the photocurrent was monitored as a function of the chopping frequency ν (Hz), however, yielded results at variance with the photoemission model introduced above. In particular, for our experimental arrangement, the RC constant of the cell with the potentiostat was less than 1 ms, and R_{far} was much larger than the sum of the solution resistance and the resistance between the working electrode and ground. Under these conditions, j_{ph} should be independent of ν up to several hundred Hertz.[6] Contrary to this expectation, j_{ph} was found to decrease markedly with increasing ν (open circles, left ordinate, Figure 3). This latter behavior prompted us to examine other possible mechanisms as responsible for the observed photoinduced currents, and, particularly, heating effects.

As shown by Benderski and Velichko[17] for a one-dimensional system, the temperature increase at the interface (ΔT) owing to an infinitely thin heat source present therein is given by

$$\Delta T = \frac{LS(1-R)}{\sqrt{\pi\chi c\rho}}\left(1+\sqrt{\frac{\chi_1 c_1 \rho_1}{\chi c \rho}}\right)^{-1}\int_0^1 \frac{f(t')}{(t-t')^{1/2}}\,dt' \quad (1)$$

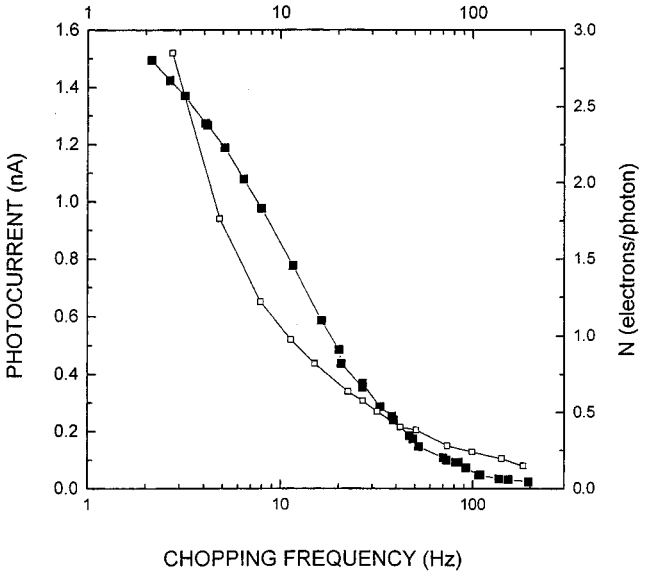

Figure 3. Comparison of X-ray (solid squares) and laser (open squares) induced heating photocurrents (see text for details) as a function of the chopping frequency.

In this equation, L is the peak power and $f(t)$ the normalized shape of the incident radiation as a function of time t, R is the reflectance, and χ and χ_1, c and c_1, and ρ and ρ_1, are the heat conductances, heat capacitances, and densities of the metal and solution, respectively. The parameter S introduced in this equation accounts for the fact that not all of the absorbed power is converted into heat due to fluorescence and other factors, an effect that has no analogue in the UV−visible spectral region. This model is valid provided that the absorption length, μ, is much smaller than the heat transfer length ($\lambda = (\chi/2c\rho\nu)^{1/2}$), which, in turn, is smaller than the dimensions of the electrode (δ); hence, it may not be strictly applicable in our case, because, even though μ (3 μm) $\ll \lambda$ (ca. 1 mm in the chopping frequency range employed), $\lambda \approx \delta$ (vide supra). Nevertheless, this formula is useful for estimating the temperature increase (ΔT) in our experiments. In particular, for $R = 0$ and $S = 1$, $L = 12$ keV $\times$ 2×10^{11} photons/cm^2 s, and $t = 1$ s

$$\Delta T = 3.39 \times 10^{-18} \frac{\mathrm{K\ cm^2\ s^{1/2}}}{\mathrm{eV}} L\sqrt{t} = 1.4 \times 10^{-3}\ \mathrm{K} \quad (2)$$

From eq 1, the heat transfer impedance in the frequency domain is given by

$$\tilde{T}(\nu) = u\frac{1-i}{2\sqrt{\nu}}\tilde{f}(\nu) \quad (3)$$

where u is the preintegral factor in eq 1.

A change in temperature at the metal−solution interface could induce heating currents, either through the temperature dependence of the double layer capacitance (C), or of the faradaic resistance (R_{far}). In the first case, the photothermal current may be expressed in the frequency domain as follows:

$$j_c(\nu) = 2\nu i C \Phi \tilde{T}(\nu) = \tilde{Z}_c \tilde{Z}_T \tilde{f}(\nu) \quad (4)$$

where Φ is the "temperature coefficient of the potential drop" across the interface.[17] Figure 4(left ordinate) shows a plot of the predicted photothermal charging current as a function of ν for typical values of C and Φ, taking into account the area of the electrode employed in this work. The charging heating currents are proportional to dΔT/dt and, therefore, increase with ν, a behavior not compatible with the experimental observations.

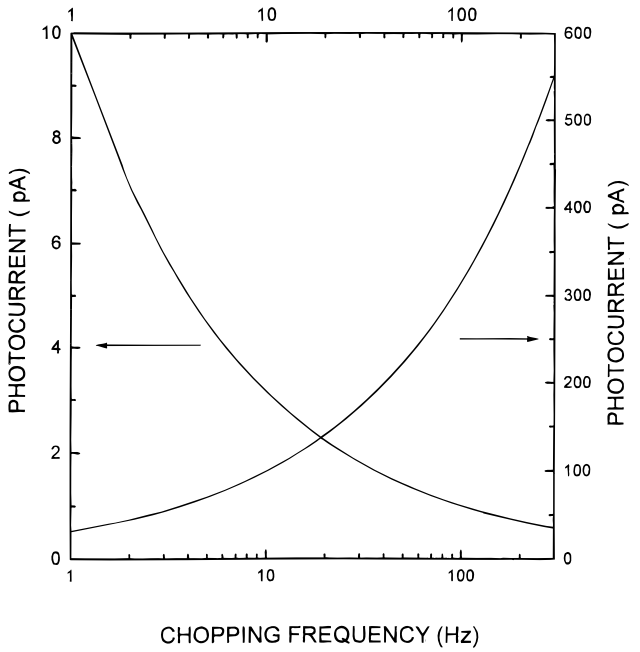

Figure 4. Plots of photothermal charging ($C = 10$ μF/cm^2, $\Phi = 1$ mV/K, left ordinate) and faradaic ($\alpha = 0.5$, $\eta = 1.3$ V, $j_{dc} = 0.75$ μA, $T = 300$ K and $kT/e = 25$ mV, right ordinate) currents as a function of ν. Electrode area (2.5 mm^2), $\tilde{T}$ is given in eq 3.

On the other hand, heating currents due to the modulation of the faradaic resistance, would be proportional to ΔT itself. In particular, the first-order term of the Maclaurin series expansion of the Butler−Volmer equation[18] with respect to temperature leads to the following expression[6]

$$\tilde{j}_P(\upsilon) = \frac{\alpha e \eta}{k\mathrm{T}} j_{dc} \frac{\tilde{T}}{T} \quad (5)$$

where α is the transfer coefficient, η the applied overpotential, k Boltzmann's constant, j_{dc} the dc dark current and T the absolute temperature. Estimates of the magnitude of the thermally modulated photocurrent $\tilde{j}_P(\upsilon)$ based on this expression (see right ordinate, Figure 4) were made using $\alpha = 0.5$, $\eta = 1.3$ V, based on the standard redox potential of the persulfate/sulfate couple, i.e., 2.010 V vs SHE,[19] and the experimentally observed value of j_{dc}, i.e., 0.75 μA. This model indeed agrees qualitatively with the experimental results; i.e., the photoinduced current decreases with frequency (Figures 3 and 4, right ordinate). Deviations of j_{ph} from the expected $\nu^{-1/2}$ dependence in the low-frequency range observed in the experimental data (see open circles in Figure 3) may be ascribed to edge effects; i.e., the heat transfer length becomes comparable to the electrode dimensions. However, the magnitude of the observed ac photocurrents, as shown in Figure 3, was about 0.7 nA at ca. 12 000 eV, which is about 2 orders of magnitude higher than that estimated from eq 5 at 6.1 Hz, i.e., 0.007 nA. At least three factors may account for this disparity: uncertainties in the values of the parameters used in eqs 2 and 5, inadequacies of eq 5 at low frequencies, or contributions to the signal arising from photocurrent sources other than those included in the present model.

Support for a temperature modulation of the faradaic current as being responsible for the observed photoeffects was obtained from experiments in which a laser beam (continuous wave Ar^+ laser, wavelength 514 nm and power 500 mW) was used to irradiate the same electrode under the same conditions involved

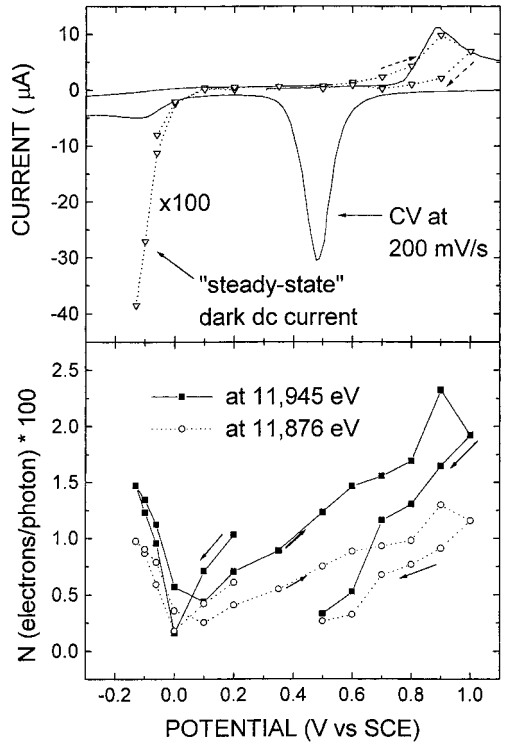

Figure 5. Upper panel: cyclic voltammogram (solid line) and "steady state" dark currents (open triangles) of the Au wire electrode in 0.50 M sodium phosphate buffer (pH = 6.72) at 200 mV/s obtained in the cell where the photoemission experiments were carried out. Lower panel: effective number of photoelectrons per incident photon, *N*, as a function of electrode potential for X-ray energies below (at 11 876 eV, open circles) and above (at 11 945 eV, solid squares) the Au L_{III} absorption edge.

in the X-ray experiments (see solid line, right ordinate, Figure 3), except that the beam did not fill the entire electrode. Since electron photoemission is not possible for the selected values of the laser wavelength and electrode potential,[6−8] the ac current can only be attributed to heating effects. Although the trends of the two sets of experimental data were similar, quantitative agreement should not be expected since, contrary to the X-ray case, the laser beam did not fill the entire electrode.

Also consistent with this faradaic heating model was the dependence of *N* on electrode potential. The upper panel, Figure 5, shows the cyclic voltammetry of Au in air-saturated phosphate buffer (solid curve) along with dc currents obtained after 1 min polarization at the various specified potentials (open triangles) during acquisition of ac data under X-ray illumination. The cathodic currents at negative potentials are due to oxygen reduction,[20] whereas the anodic currents are due to gold oxide formation.[9] Note that this latter process occurs with significant hysteresis due its slow kinetics.[9] The amplitude of *N*, shown in the lower panel, increases with a corresponding increase in the dc current as should be expected based on eq 8. In particular, it becomes negligible at 0.0 V vs SCE, a potential at which the dc current changes sign, and tracks qualitatively the hysteretic behavior in the anodic potential region described above. It should be emphasized that unlike UV−visible induced photoemission, for which there is a threshold that depends on the energy of incident photon and the applied electrode potential, the X-ray induced photoemission is expected to have no potential dependence. It becomes evident by comparing Figures 2 and 5, that the photocurrents observed for the Au electrode polarized at 0.5 V vs SCE increase by 2 orders of magnitude upon addition of persulfate into the solution. Since persulfate can be reduced at this potential, albeit at a small rate,[21] it produces a larger dark dc current and, thus, by virtue of eq 5, a larger temperature-modulated signal.

The edge jump ratio obtained from the results shown in Figure 5 (1.6 ± 0.1) is within the range observed in other experiments (see Discussion of Figure 2). Since the reflectance under the nongrazing incidence angle conditions employed in this study is essentially zero, ca. $10^{-10}-10^{-19}$ (ref 22), ΔT depends on the X-ray energy only via *S*. Values of *S* above and below the Au L_{III} absorption edge were calculated by assuming that only primary fluorescence into 2π sterad angle[23] leads to a loss of absorbed power. After accounting for self-absorption effects, the magnitude of PCA EJR was found to be 0.55, and, thus, smaller than one. This result can be readily rationalized based on the fact that in the case of Au, the self-absorption of the M-fluorescence photons with energies of ca. 2 keV is significant, whereas the opening of the new L-fluorescence channel above the edge produces 10 keV photons which can easily escape carrying energy away from the specimen. This discrepancy between the experimentally found EJR and that predicted by the heating model certainly deserves further study.

Conclusions

The experimental results presented in this work have demonstrated that the photocurrents generated at metal/solution interfaces as a function of the energy of the incident X-rays around the Au L_{III} absorption edge display striking similarities to the X-ray absorption near edge structure acquired by more conventional means. Two mechanisms were considered to explain the origin of the photocurrents: photoelectron emission and temperature-induced modulation of the faradaic current across the interface. Although the magnitude of the photocurrent above the Au L_{III}-edge (up to 1 electron per incident photon, or 280 pA/mm^2) appears consistent with both mechanisms, the observed dependence of the X-ray-induced photocurrents on the chopping frequency and electrode potential is in agreement with heating, rather than photoelectron emission, as the primary phenomenon responsible for the measured effects. Specifically, the photocurrent amplitude was found to decrease with ν and to change monotonically with the magnitude of the dark dc current. It is likely that pure photoemission currents could be detected at chopping frequencies high enough for temperature effect variations at the interface to be significantly reduced. No satisfactory account could be made, within either one of these models, for the fact that the observed magnitude of the edge jump ratio (EJR) was close to the absorption cross section EJR.

Insight into the role of heating following X-ray photon absorption could be gained by photoacoustic[24] and beam deflection[25] detection as well as measurements of equilibrium redox potentials.[26] Experiments of this type are currently being considered in this laboratory.

Acknowledgment. This work was funded in part by the U.S. Department of Energy, Office of Basic Energy Sciences. We would like to acknowledge enlightening discussions with Dr. E. Gullikson and Dr. T. Rabedeau of SSRL regarding X-ray reflectance and relationships between X-ray absorbance and heating.

References and Notes

(1) Chu, Y. S.; You, H.; Tanzer, J. A.; Lister, T. E.; Nagy, Z. *Phys. Rev. Lett.* **1999**, *83*, 552.

(2) Resonance X-ray scattering from Pt(111)-surfaces under water. You, H.; Chu, Y. S.; Lister, T. E.; Nagy, Z.; Ankudiniv, A. L.; Rehr, J. J. *Physica* **2000**, *B283*, 212.

(3) See for example: Toney, M. F.; Melroy, O. R. In *Electrochemical Interfaces: Modern Techniques for in-situ Interface Characterization*; Abruna, H. D., Ed.; VCH Publishers: New York, 1991.
(4) Hansen, G. A.; O'Grady, W. E. *Rev. Sci. Instrum.* **1990**, *61*, 2127.
(5) Stohr, J. In *X-ray absorption: principles, applications, techniques of EXAFS, SEXAFS, and XANES*; Koningsberger, D. C., Prins, R., Eds.; Wiley: New York, 1988.
(6) Benderskii, V. A.; Brodskii, A. M. In *Fotoemissiya iz Metallov v Rastvory Elektrolitov*; Nauka: Moscow, 1977.
(7) Benderskii, V. A.; Benderskii, A. V. *Laser Electrochemistry of Intermediates*; CRC Press: Boca Raton, FL, 1995.
(8) Gurevich, Y. Y.; Pleskov, Y. V.; Rotenberg, Z. A. In *Photoelectrochemistry*; Consultant Bureau: New York, 1980.
(9) Angerstein-Kozlowska, H.; Conway, B. E.; Hamelin, A.; Stoicoviciu, L. *Electrochim. Acta* **1986**, *31*, 1051.
(10) Schroeder, S. L. M.; Moggridge, G. D.; Ormerod, R. M.; Lambert, R. M.; Rayment, T. *Physica B* **1995**, *208 & 209*, 215.
(11) Nagy, Z.; You, H. *J. Electroanal. Chem.* **1995**, *381*, 275.
(12) Kordesh, M. E.; Hoffman, R. W. *Phys. Rev. B* **1984**, *29*, 491.
(13) Song, I.; Rickett, B.; Janavicius, P.; Payer, J. H.; Antonio, M. R. *Nucl. Instrum. Methods A* ***1995***, *360*, 634.
(14) See, for example: Goulon, J.; Goulon-Ginet, C.; Cortes, R.; Dubois, J. M. *J. Physique* **1982**, *43*, 539. Tan, Z.; Budnick, J. I.; Heald, S. M. *Rev. Sci. Instrum.* **1989**, *60*, 1021.
(15) Bertin, E. P. *Principles and Practise of Quantitative X-ray Fluorescence Analysis*, 2nd ed.; Plenum Press: New York, 1975.
(16) Watanabe, T.; Gerischer, H. *J. Electroanal. Chem.* **1981**, *117*, 185 and references therein.
(17) Benderskii, V. A.; Velichko, G. I. *J. Electroanal. Chem.* **1982**, *140*, 1.
(18) Schmickler, W. In *Interfacial Electrochemistry*; Oxford University Press: New York, 1996.
(19) *CRC Handbook of Chemistry and Physics*, 80th ed.; Lide, D. R., Ed.; CRC Press: Boca Raton, FL, 1999.
(20) Zurilla, R. W.; Chen, R. K.; Yeager, E. *J. Electrochem. Soc.* **1987**, *125*, 11036.
(21) Samec, Z.; Doblhofer, K. *J. Electroanal. Chem.* **1996**, *409*, 165.
(22) Henke, B. L.; Gullikson, E. M.; Davis, J. C. X-ray interactions: photoabsorption, scattering, transmission, and reflection at $E = 50-30000$ eV, $Z = 1-92$. *Atomic Data and Nuclear Data Tables, July* **1993**, *54* (no.2): 181−342; http://www-cxro.lbl.gov/optical_constants/.
(23) Jenkins, R.; Gould, R. W.; Gedeke, D. *Quantitative X-ray Spectrometry*, 2nd ed.; Marcel Dekker: New York, 1995.
(24) Reichling, M.; Masujima, T.; Shiwaku, H.; Kawata, H.; Ando, M.; Matthias, E. *Appl. Phys. A* **1989**, *49*, 707. Masujima, T.; Shiwaku, H.; Yosihda, H.; Kataoka, M.; Reichling, M.; Imai, H.; Katawa, H.; Iida, A.; Koyama, A.; Ando, M. *Jpn. J. Appl. Phys.* **1989**, *28*, L513. Toyoda, T.; Masujuma, T.; Ando, M. *Jpn. J. Appl. Phys.* **1993**, *32*, 2550.
(25) Rudnicki, J. D.; McLarnon, F. R.; Cairns, E. J. In *Techniques for Characterization of Electrodes and Electrochemical Processes*; Varma, R., Selman, J. R., Eds.; Wiley: New York, 1991.
(26) Valdes J. L.; Miller, B. *J. Electrochem. Soc.* **1988**, *92*, 4483.